Journal of Physical Science, Vol. 35(3), 65–80, 2024

Phosphorus Activation via Screen Printing Ag/P on Thermally Grown SiO_2 Layer as Passivating Contact on n-Si

Ahmad Rujhan Mohd Rais,[1*] Nurul Aqidah Mohd Sinin,[2] Muhammad Hatim Rohaizar,[2] Mohd Adib Ibrahim,[2] Kamaruzzaman Sopian[3] and Suhaila Sepeai[2*]

[1]School of Physics, Universiti Sains Malaysia, 11800 USM, Pulau Pinang, Malaysia
[2]Solar Energy Research Institute, Universiti Kebangsaan Malaysia, 43600 Bangi, Selangor, Malaysia
[3]Department of Mechanical Engineering, Universiti Teknologi PETRONAS, 32610 Seri Iskandar, Perak, Malaysia

Corresponding Author: rujhanrais@usm.my, suhailas@ukm.edu.my

Published online: 31 December 2024

To cite this article: Mohd Rais, A. R. et al. (2024). Phosphorus activation via screen printing Ag/P on thermally grown SiO_2 layer as passivating contact on n-Si. *J. Phys. Sci.*, 35(3), 65–80. https://doi.org/10.21315/jps2024.35.3.5

To link this article: https://doi.org/10.21315/jps2024.35.3.5

ABSTRACT: *This research investigates the impact of screen printing silver (Ag) with phosphoric acid (H_3PO_4) as a metallic dopant paste on etched versus non-etched thermally grown silicon dioxide (SiO_2) layers used as passivating contacts in silicon solar cells. The combination of Ag and phosphorous (P) from H_3PO_4 is denoted as Ag/P metallic dopant paste. Passivating contacts are crucial for reducing recombination losses and improving solar cell efficiency. Thermally grown SiO_2 layers are commonly used due to their excellent passivation properties and compatibility with silicon substrates. The study involves a comprehensive comparison of the performance of etched and non-etched SiO_2 layers, including the activation of P from H_3PO_4 and series resistance. The methodology involves the thermal growth of SiO_2 layers on silicon wafers, followed by selective etching on a subset of the samples. Subsequently, Ag/P is deposited on both etched and non-etched SiO_2 layers using the screen printing technique. The samples undergo annealing using a round quartz furnace to form the passivating contacts. The dark current-voltage measurements are employed to evaluate the activation of P, series resistance and the behaviour of the screen-printed n-type silicon (n-Si). The results reveal the activation of P from Ag/P when adding more H_3PO_4 with Ag paste. The etched SiO_2 layers also exhibited lower total current and an onset between semi-ohmic and ohmic behaviour. Meanwhile, the Ag and Ag/P screen-printed on SiO_2 layers revealed higher total current but exhibited an onset between leaky-diode and ohmic behaviour. Specifically, the etched SiO_2 layers demonstrated improved surface passivation quality, evidenced by lower surface recombination velocities.*

Keywords: dopant paste, etched SiO_2, passivating contact, phosphorus activation, silicon

1. INTRODUCTION

Solar cell technology has witnessed significant progress in the past few decades, driven by the global demand for sustainable energy solutions. Passivating contacts hold a crucial position among the key components that shape the performance and efficiency of solar cells. These contacts play a vital role in reducing recombination losses by effectively passivating the surface states that can trap charge carriers, thereby boosting the solar cell's overall efficiency. Among various materials, silver (Ag), polysilicon (poly-Si), phosphorus oxychloride ($POCl_3$) and boron tribromide (BBr_3) as dopant sources on thermally grown silicon dioxide (SiO_2) layers have emerged as a promising approach for forming efficient passivating contacts.

SiO_2 has emerged as adequate passivating layers due to their ability to form high-quality interfaces with Si substrates. SiO_2 layers, typically formed through controlled oxidation processes, provide excellent surface passivation by reducing interface defect states and minimising carrier recombination. These properties enhance Si solar cells' practical carrier lifetime and open-circuit voltage (V_{OC}). Besides that, SiO_2 is one of the important components in passivating contact. These layers are essential for reducing charge carrier recombination at the Si surface, thereby enhancing the efficiency of solar cells. In addition, SiO_2 layers significantly reduce charge carrier recombination at the Si surface, which is vital for high-efficiency Si solar cells.[1–3] Ultra-thin SiO_2 layers can be deposited under high temperature and low-pressure conditions, maintaining their electronic properties up to 900°C, making them compatible with existing industrial processes.[2] Furthermore, strong impurity gettering is one of the major effects of doped poly-Si passivating contacts with SiO_2 layers, which will help redistribute impurities away from the Si wafer bulk.[4] These layers have been fundamental in both historical and modern advancements in photovoltaic technology, contributing to the development of high-efficiency solar cells.

The usage of $POCl_3$ and BBr_3 as dopant sources has shown considerable promise in creating passivating contacts on Si-based solar cells. Doping is a critical process in fabricating Si-based solar cells, as it introduces impurities into the Si to modify its electrical properties, creating regions of n-type or p-type material. These dopant sources are commonly used on the poly-Si layer to create n^+-poly-Si and p^+-poly-Si layers, respectively. Both processes yield high uniformity, which is crucial for high-efficiency Si-based solar cells.[5–9] However, both processes have drawbacks, such as high thermal budgets and environmental concerns. Both $POCl_3$ and BBr_3 diffusion require high temperatures, which can increase energy consumption and potential thermal degradation of the Si wafers. The formation of a boron layer requires a higher temperature process than the phosphorous (P)

dopant process, which will degrade the carrier lifetime in the bulk of Si wafer.[10,11] Thus, this necessitates careful thermal management to prevent damage and maintain wafer integrity. $POCl_3$ and BBr_3 are highly corrosive and toxic, posing safety and environmental challenges during handling and processing. This is due to gaseous phosphorus pentoxide (P_2O_2) and chlorine (Cl_2), which are produced from the $POCl_3$ diffusion process and are harmful to human health and the environment.[12,13] In addition, the boron-rich layer (BRL) is a toxic and harmful chemical that affects the low yield in mass production due to its side effects on humans and the environment.[14] Therefore, phosphoric acid (H_3PO_4) will be an alternative approach for conventional dopant sources formation on Si wafers that will be less toxic and harmful to humans. The application of H_3PO_4 as an n^+ dopant source on n-Si wafers has been studied by experiment and simulation in previous studies that show a promising results.[15,16]

This paper focuses on combining screen-printing dopants with metallic paste, which was created by mixing Ag and H_3PO_4 solution, known as silver phosphorous (Ag/P) metallic dopant paste. This paste will undergo a single screen-printing process and an in-situ annealing process. The Ag/P serves two purposes: to create emitters and metallic contacts on the Si solar cell in one process. This idea was created based on current approaches of screen printing dopants for uniform diffusion of dopants on Si wafers. The idea of Ag/P metallic dopant paste comes from the selective emitter (SE) process. In conjunction, the homogenous sheet resistance across the Si wafer will be achieved using the screen-printing dopant method.[17] In summary, the optimisation of passivating contacts on n-Si wafers involves a careful balance of surface treatments, doping methods and passivating layers. The integration of SiO_2 with metallic dopant paste of Ag and H_3PO_4 contacts offers a multifaceted approach to achieving high-efficiency solar cells.

2. EXPERIMENTAL

The starting wafer used for fabrication is a polished n-type mono-crystalline wafer with a thickness of 200 μm. The polished n-Si wafers were cleaned by immersing them in heated acetone, steeping them in methanol and then rinsed with deionised (DI) water. The additional steps of cleaning process using the mixture of DI water (H_2O): ammonium hydroxide (NH_4OH): hydrogen peroxide (H_2O_2) with a ratio of 5:1:1 DI water and NH_4OH have been conducted and rinsed with DI water along with drying process by suing nitrogen gas (N_2). Then, all samples will be oxidised inside a round quartz furnace for a wet thermal oxidation process. After the oxidation process, a one-sided oxidation layer on the n-Si wafers was removed using hydrofluoric acid (HF) vapour. The entire samples with etched and non-etched SiO_2 layers on the rear have been categorised in Table 1 and

Figure 1. The oxidation process inside a round quartz furnace for wet thermal oxidation was conducted in Solar Energy Research Institute (SERI), Universiti Kebangsaan Malaysia (UKM).

Table 1: Description of the devices with etched and no-etched SiO_2 layers on the rear

Description of the devices				
Wafer	SiO_2 layer on the front surface	SiO_2 layer on the rear surface	Metallic paste used on the front surface	Metallic paste used on the rear surface
n-Si	Non-etched	Non-etched	Ag	Ag
		Etched	Ag	Al
		Non-etched	5% Ag/P	5% Ag/P
		Etched	5% Ag/P	Al
		Non-etched	7.5% Ag/P	7.5% Ag/P
		Etched	7.5% Ag/P	Al
		Non-etched	10% Ag/P	10% Ag/P
		Etched	10% Ag/P	Al

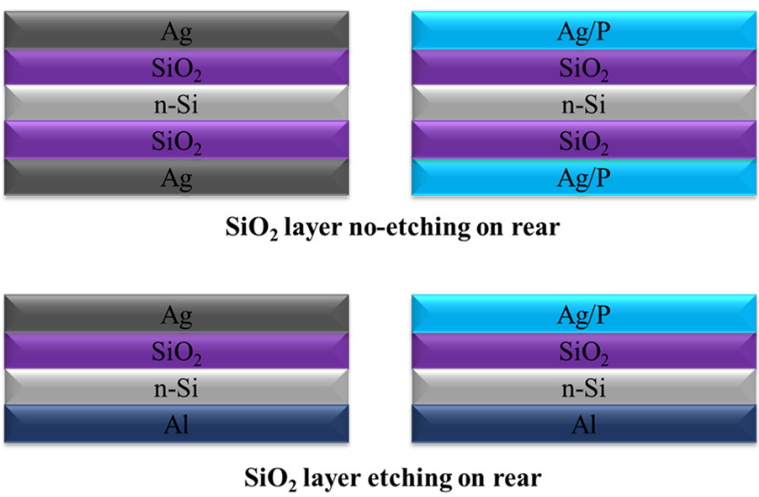

Figure 1: Structure of n-Si screen-printed with Ag and Ag/P on etched or non-etched SiO_2 layer on the rear.

This work has prepared the combination of Ag paste and H_3PO_4 as an Ag/P metallic dopant paste. This process was prepared by mixing fixed 10 g of Ag paste with a variation amount of pure H_3PO_4 solution. Table 2 presents the ratio of Ag and H_3PO_4 used for the variation Ag/P concentration. The annealing process took place inside the 4-inch round quartz furnace provided by SERI, UKM.

Table 2: The preparation of Ag/P

Silver paste, Ag (grams)	Phosphoric acid, H_3PO_4 (grams)	Ag/P (%)
10	0.5	5
10	0.75	7.5
10	1	10

The application of a new metallic dopant paste of Ag/P dopant paste is being conducted on n-Si wafers with an in-situ process of SiO_2 and excess $POCl_3$ inside the round quartz furnace. This is due to a study of the effectiveness of P doping with Ag paste on the Si substrate via contact resistance inferred from diode current-voltage (I-V). The n-Si wafers with both surfaces coated with SiO_2 are screen-printed with Ag/P paste for both surfaces. Meanwhile, n-Si with SiO_2 etched at the rear side is screen-printed with Al at the rear surface and Ag/P at the front. The process took place using a 4-inch quartz furnace with 45 s in, variable holding time (30 s, 50 s, 70 s, 90 s, 110 s) and 45 s out at 900ºC. Table 1 explains the details of the devices used in this paper.

The dark current-voltage (DI-V) curve of a semiconductor device shows the current through the device as a function of the applied voltage when there is no illumination (dark conditions). This characterisation method provides information such as series resistance to assess junction, grid and contact resistance. The exponential graph in the form of a diode is plotted by the DI-V, which provides the current and voltage in dark conditions. According to the plotted graph, the series resistance can be estimated, and the behaviour of the devices can be classified. The equipment and methods used to determine series resistance from dark I-V measurements are the same as the procedure discussed in the chapter "Dark Current-Voltage Characterisation" published in Crystalline Silicon Solar Cells and previous research on concentration factor on the mixture of Ag paste and H_3PO_4 solution as a dopant paste for contact formation in silicon solar cells.[16,18] Most of the characterisation processes were conducted in SERI, UKM.

3. RESULTS AND DISCUSSION

Based on all data presented and discussed in this section, a metallic paste combined with water-based H_3PO_4 was demonstrated. This section focuses on the Ag/P dopant paste as an alternative to a single metallic-dopant paste and passivating contact for Si solar cells, respectively. The proposed method is particularly relevant as it allows for the simultaneous creation of metallic contact and emitter region on the Si wafer, a crucial step in solar cell manufacturing.

The formation of screen-printed Ag, 5% Ag/P (Ag/P5) and 10% Ag/P (Ag/P10) on n-Si wafers has been analysed using a field emission scanning electron microscope (FESEM) for front view evaluation. Figure 2 illustrates the top view from a FESEM on Ag screen-printed Ag/P5 and Ag/P10 after annealing at 900ºC for 40 s holding time inside a round quartz furnace. As shown in Figure 2(a), the baseline Ag screen-printed on n-Si formed an almost smooth screen-printed metallic paste compared with Ag/P5 and Ag/P10. The addition of P from H_3PO_4 introduced some additional structures or roughness from P particles, significantly altering the smoothness of the screen-printed metallic dopant paste. The different hollow gaps between Ag/P10 with baseline Ag and Ag/P5 are significant when increasing P on Ag/P dopant paste as the quantity of H_3PO_4 is increased when mixed with pure Ag metallic paste. In conjunction, at the right amount of Ag paste and H_3PO_4, the P particles will be well mixed with Ag paste. Hence, P particles are activated and reacted with Ag paste and n-Si as emitters and metallic contacts, which increase the conductivity of the Ag paste and form an n+ emitter junction along with the metallic finger contacts. These findings have significant implications for the conductivity and junction formation in the Ag paste, providing a deeper understanding of the role of P addition in the properties of the screen-printed metallic dopant paste.

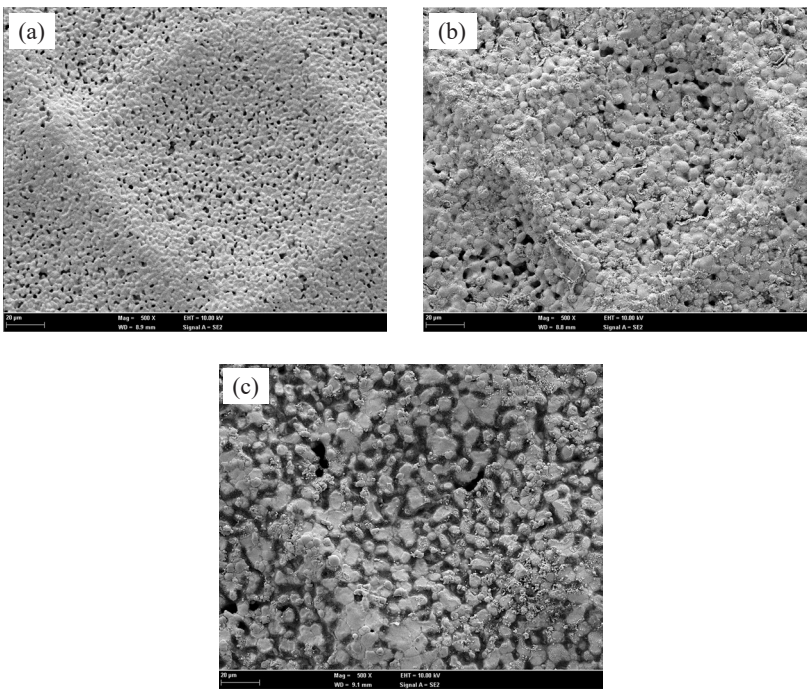

Figure 2: FESEM images of top view on screen printed (a) Ag as the baseline, (b) Ag/P5 and (c) Ag/P10.

The electrical properties of screen-printed Ag, Ag/P5, 7.5% Ag/P (Ag/P7.5) and Ag/P10 on n-Si wafers have been investigated under no illumination by dark I-V evaluation measurement. Figure 3 indicates the dark I-V evaluation on the n-Si wafer with an oxide layer on both the front and rear surface screen-printed with Ag, Ag/P5, Ag/P7.5 and Ag/P10 on the rear with different annealing holding times at the same temperature. Annealing of Ag/P10 paste at a holding time of 30 s resulted from low R_s and more ohmic behaviour than Ag/P7.5. At the same time, Ag/P5 and Ag baseline are leaky diodes that do not show any resistance between metallic contacts and Si. Furthermore, increasing the holding time to 50 s, 70 s and 110 s shows the dominance of Ag/P7.5 metallic dopant paste over Ag/P10 in R_s and ohmic behaviour. In contrast, Ag/P5 dopant paste exhibits higher R_s and behaves almost like a leaky diode throughout the annealing process's 30 s–110 s holding time. However, at 90 s holding time, the Ag baseline has the lowest R_s than Ag/P5, Ag/P7.5 and Ag/P10. Metallic dopant pastes of Ag/P7.5 and Ag/P10 still have low R_s for 90 s compared to Ag/P5. Other than that, the mixture of Ag/P5 is not easily screen-printed on n-Si as the paste becomes hardened. Concentration lightly under the rear metal shows some recombination velocity due to increasing contact resistance and leakage current.

The combination of intermediate SiO_2 under a thin coating of highly doped Si makes the electrical current flow out of the cell with almost zero losses.[19] As discussed, the in-situ process of thermally grown SiO_2 with excess $POCl_3$ inside a quartz furnace is annealed on the n-Si for evaluation in this section. The mechanism of the passivated emitter and rear cell (PERC) with passivated oxide SiO_2 layer at the rear explained an improvement of the short circuit current density (J_{SC}) and V_{OC} due to a reduction in surface recombination at the rear surface. Other than that, the Si-SiO_2 interface features low-interface state density (D_{it}) and captures cross-sections, which are highly asymmetric and have low-positive fixed charge density (Q_f) are major for the electrical properties characterisation of dielectric passivation layers by SiO_2.[1]

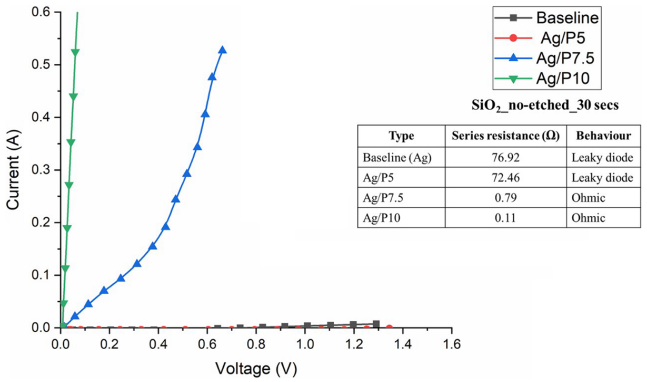

SiO_2_no-etched_30 secs

Type	Series resistance (Ω)	Behaviour
Baseline (Ag)	76.92	Leaky diode
Ag/P5	72.46	Leaky diode
Ag/P7.5	0.79	Ohmic
Ag/P10	0.11	Ohmic

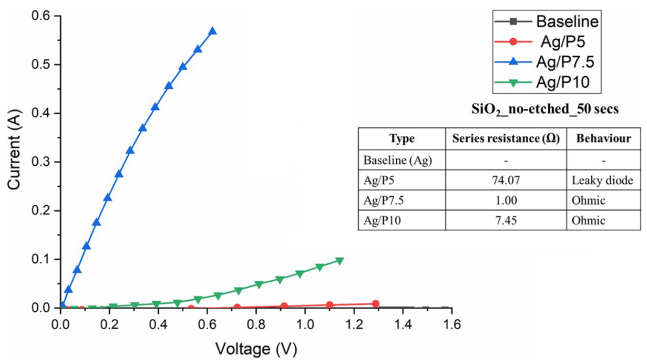

SiO_2_no-etched_50 secs

Type	Series resistance (Ω)	Behaviour
Baseline (Ag)	-	-
Ag/P5	74.07	Leaky diode
Ag/P7.5	1.00	Ohmic
Ag/P10	7.45	Ohmic

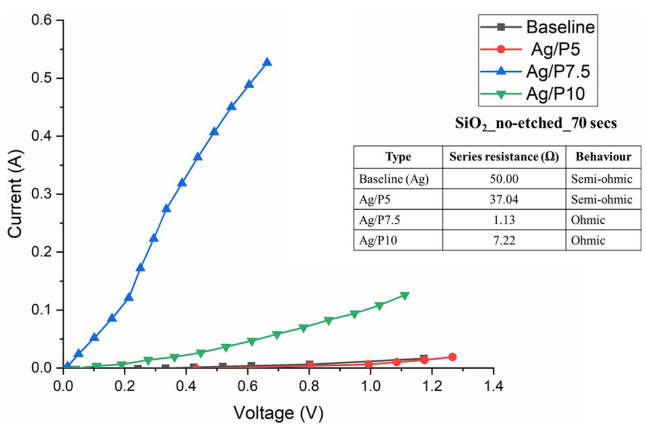

SiO_2_no-etched_70 secs

Type	Series resistance (Ω)	Behaviour
Baseline (Ag)	50.00	Semi-ohmic
Ag/P5	37.04	Semi-ohmic
Ag/P7.5	1.13	Ohmic
Ag/P10	7.22	Ohmic

Figure 3: Dark I-V evaluation of no-etched oxide layer (SiO_2) on the rear screen printed with Ag, Ag/P5, Ag/P7.5 and Ag/P10 on both surfaces of n-Si with the variation of annealing time in s (*continued on next page*).

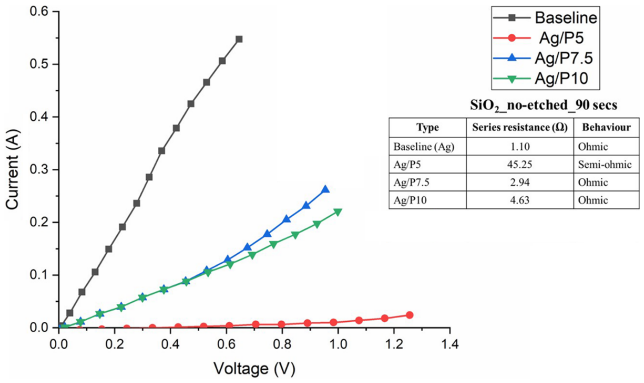

SiO_2_no-etched_90 secs

Type	Series resistance (Ω)	Behaviour
Baseline (Ag)	1.10	Ohmic
Ag/P5	45.25	Semi-ohmic
Ag/P7.5	2.94	Ohmic
Ag/P10	4.63	Ohmic

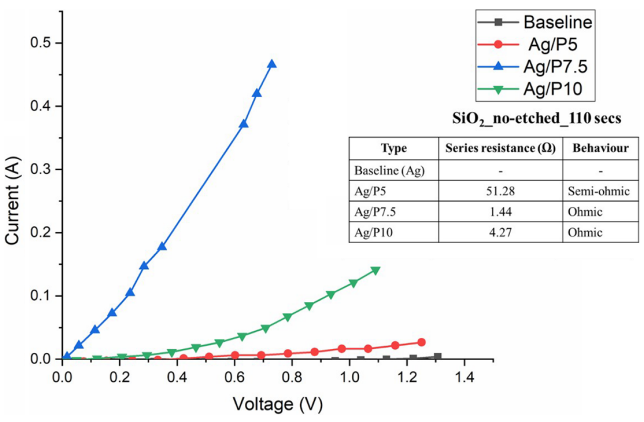

SiO_2_no-etched_110 secs

Type	Series resistance (Ω)	Behaviour
Baseline (Ag)	-	-
Ag/P5	51.28	Semi-ohmic
Ag/P7.5	1.44	Ohmic
Ag/P10	4.27	Ohmic

Figure 3: (*Continued*).

Figure 4 illustrates the dark I-V evaluation on the n-Si wafer with an oxide layer etched on the rear screen-printed with only aluminum (Al) paste, and the front surface is screen-printed with Ag, Ag/P5, Ag/P7.5 and Ag/P10 with different annealing holding time at the same temperature. Note that all n-Si screen-printed with Ag/P7.5 on the front surface and Al on the rear indicates the lowest R_s than other metallic pastes for all variations of annealing holding time, followed by Ag/P10 for all annealing holding times except for 70 s. At 70 s holding time, Ag/P5 shows a better R_s than Ag and Ag/P10 metallic dopant paste. Meanwhile, Ag/P5 has a larger R_s than Ag/P7.5 and Ag/P10 metallic dopant paste. Based on Figure 4, the Ag screen-printed on n-Si indicates the highest R_s compared to Ag/P metallic dopant paste. According to Figure 3, samples screen-printed with Ag, Ag/P5, Ag/P7.5 and Ag/P10 on the oxide layer at the rear n-Si show the lowest R_s than the Al screen-printed on the etched oxide layer at the rear surface. This is due to more shunting occurring because of leakage current.

Other than that, samples with an oxide layer on the rear screen printed with Ag/P paste show an improvement in shunting compared to an etched oxide layer on the rear due to low leakage current. In conjunction with that, the oxide layer has the potential to enhance resistance toward recombination at the metal interface. At the same time, it utilises the work junction difference between the metal contact and Si in most semiconductors to be more efficient, thereby inducing an effective junction. Furthermore, surface recombination velocity (S) is lower for n-Si due to the electron and hole capture cross-section asymmetry, making it less dependent on the excess carrier density.[20,21] However, screen-printing Ag/P7.5 on n-Si using a screen-printing mask is difficult as Ag/P5 for the paste to pass through the mask film. Thus, adding more H_3PO_4 to Ag paste to produce Ag/P10 dopant paste has been conducted.

Since the passivated emitter refers to high-quality oxide at the front surface, it significantly lowers the number of carriers recombining at the surface. Besides that, the rear is locally diffused only at the metal contacts, Ag/P, to minimise recombination at the rear while maintaining good electric contacts. Hence, the passivated emitter and rear show an advantage in enhancing the internal reflection of long-wavelength light. Apart from that, the interaction of charge carriers with defects or in-homogeneities and carrier collection probability greatly impact the current generation, especially between SiO_2/crystalline silicon (c-Si) interfaces. In addition, carrier collection efficiency is uniform for silicon oxide (SiO_x) contact and conduction activation due to the enhancement of dopant diffusion. This will produce a local depletion region under the SiO_x region, resulting in highly effective carrier separation.[22]

According to Figure 3 and Figure 4, Ag/P7.5 has the lowest R_s among other pastes. However, there is a problem during the screen-printing process using a printing mask, especially when using a small bus bar and fingers, due to the solidifying Ag/P7.5 metallic paste that has been discussed in the early part of this section. Thus, Ag/P10 paste is chosen as metallic dopant paste for full-device interdigitated back contact (IBC) Si solar cells because it is much easier to screen-print using a printing mask.

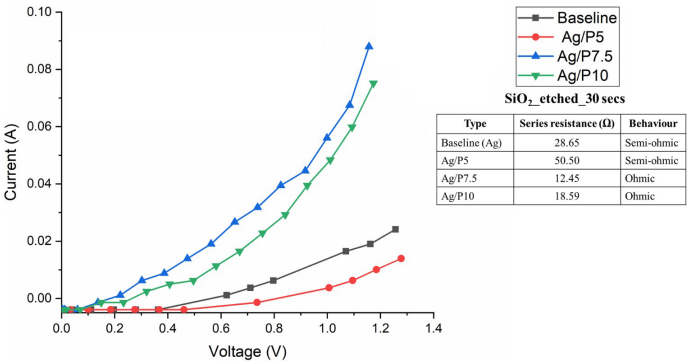

SiO_2_etched_30 secs

Type	Series resistance (Ω)	Behaviour
Baseline (Ag)	28.65	Semi-ohmic
Ag/P5	50.50	Semi-ohmic
Ag/P7.5	12.45	Ohmic
Ag/P10	18.59	Ohmic

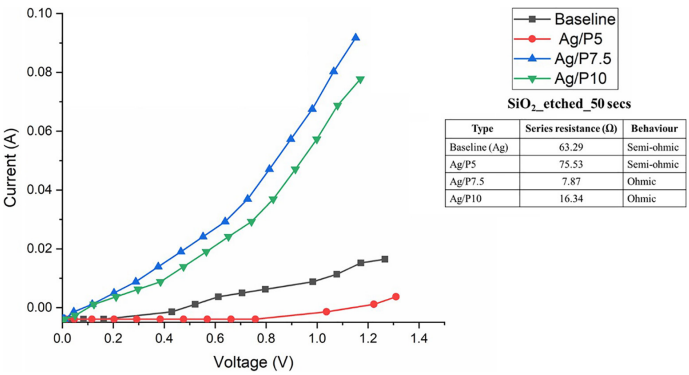

SiO_2_etched_50 secs

Type	Series resistance (Ω)	Behaviour
Baseline (Ag)	63.29	Semi-ohmic
Ag/P5	75.53	Semi-ohmic
Ag/P7.5	7.87	Ohmic
Ag/P10	16.34	Ohmic

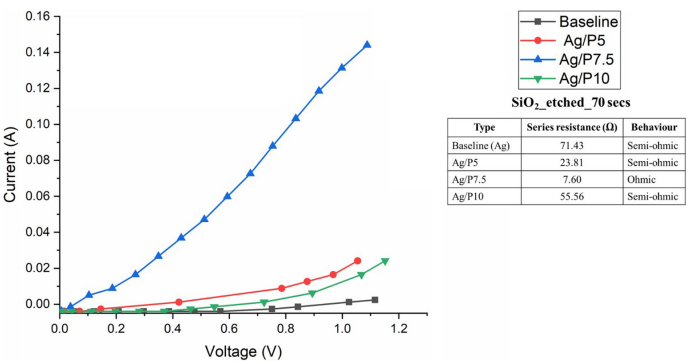

SiO_2_etched_70 secs

Type	Series resistance (Ω)	Behaviour
Baseline (Ag)	71.43	Semi-ohmic
Ag/P5	23.81	Semi-ohmic
Ag/P7.5	7.60	Ohmic
Ag/P10	55.56	Semi-ohmic

Figure 4: Dark I-V evaluation of etched oxide layer (SiO_2) on the rear screen-printed with Al and Ag, Ag/P5, Ag/P7.5 and Ag/P10 on the front surface of n-Si with the variation of annealing time in s (*continued on next page*).

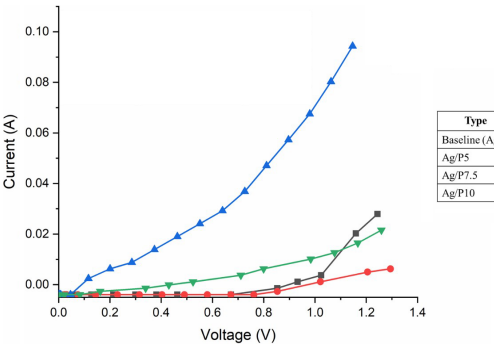

SiO_2_etched_90 secs

Type	Series resistance (Ω)	Behaviour
Baseline (Ag)	11.48	Semi-ohmic
Ag/P5	46.08	Semi-ohmic
Ag/P7.5	13.46	Ohmic
Ag/P10	37.45	Semi-ohmic

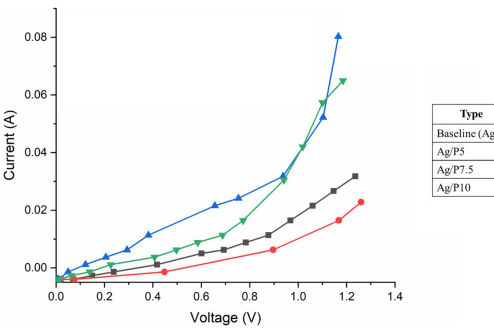

SiO_2_etched_110 secs

Type	Series resistance (Ω)	Behaviour
Baseline (Ag)	19.76	Semi-ohmic
Ag/P5	22.83	Semi-ohmic
Ag/P7.5	8.09	Ohmic
Ag/P10	8.97	Ohmic

Figure 4: (*Continued*).

Most of the baseline Ag paste metallisation, as shown in Figure 3 and Figure 4, illustrates an onset of either leaky-diode or semi-diode behaviour. This is due to the fact that no additional P is presented with metallic paste that will simultaneously be diffused into n-Si wafers. Besides that, the work function of n-Si is around 4.58 eV and Ag is 4.35 eV, which are closer to each other.[23,24] Since the work function between n-Si and Ag are close to each other, the bending of the energy band gap will be smaller between metal-semiconductors. The Schottky barrier formed from the interaction between n-Si and Ag baseline significantly impacts current transport across the barrier, depending on barrier height ($\varnothing_{bn}$) and the doping of the n-Si. In conjunction, high doping levels introduced under the metal contact layer will narrow the $\varnothing_{bn}$.[25] Therefore, the higher the doping, the narrower the Schottky barrier becomes and the lower the contact resistivity. Thus, Ag paste was improved by mixing Ag with pure H_3PO_4 solution.

Additional pure H_3PO_4 solution with Ag paste to form a metallic dopant paste of Ag/P showed an improvement toward ohmic behaviour, which is much better than for standalone Ag annealed on n-Si. This is associated with enhancing P (n-type) concentration diffused into n-Si via the co-annealing process. This refinement can

be seen when the concentration of H_3PO_4 is increased with the same amount of Ag paste quantity. This process of screen-printed Ag/P on n-Si, known as self-doped of P-doped with Ag with different types of P, showed promising results on contact resistivity and conductivity.[26,27] The significance of the activation of P can be seen when increasing the quantity of P with Ag paste. So, high doping concentration produces a narrow depletion layer as there consists of carrier tunnelling through the potential barrier, which makes it easier for electrons to make the transition.[28] Other than that, applying P using the variation of diffusion time of 10 min, 15 min and 20 min determines a significant impact on increasing and decreasing metallic contact resistance.[29]

Overall, the total current generated from the no-etched SiO_2 on n-Si was higher than the current generated by the etched SiO_2 layer. However, most of the n-Si with screen-printed Ag and Ag/P on the etched SiO_2 layer showed an onset between semi-ohmic and ohmic behaviour. Meanwhile, screen-printed Ag and Ag/P on the SiO_2 layer exhibited an onset between leaky-diode to ohmic behaviour. The reduction of interface state density by the SiO_2 layer can enhance the surface passivation of solar cells rather than using the silicon-silicon nitride (Si-SiN_x) interface. Charge fluctuation by the Si-SiO_2 interface impacts both front and rear surfaces, especially with the cell that has the most dependence on the rear surface.[30] Besides that, interfacial SiO_2 also significantly affects total negative charge concentration and is needed to build a substantial negative charge for the aluminum layer. [31–33] In addition, the Si-SiO_2 interface is able to create a huge reduction in contact recombination.

4. CONCLUSION

In conclusion, this study demonstrated that the activation of P from H_3PO_4 plays a critical role in reducing resistivity and improving ohmic contact behaviour in silicon solar cells. The diffusion of P into n-Si during the annealing process enhanced the P concentration, improving electrical performance, which can be seen for the metallic dopant paste of Ag/P7.5 and Ag/P10. Meanwhile, lightly doped areas under the rear metal contacts, such as Ag/P5, exhibited increased contact resistance and recombination velocity. High P concentrations effectively minimised recombination and contact resistance, enhancing cell efficiency. By focusing diffusion locally at the Ag/P metal contacts, we achieved better electrical contact while reducing rear-surface recombination.

5. ACKNOWLEDGEMENTS

This work was supported by a Universiti Sains Malaysia, short-term grant with project no: R501-LR-RND002-0000000210-0000. In addition, the authors would like to express many thanks to Solar Energy Research Institute, Universiti Kebangsaan Malaysia, and Dr. Saleem H. Zaidi from Gratings Incorporated, Albuquerque, New Mexico, USA, for collaboration and guidance in completing the whole process of the theoretical and experimental works.

6. REFERENCES

1. Glunz, S. W. & Feldmann, F. (2018). SiO_2 surface passivation layers – a key technology for silicon solar cells. *Sol. Energy Mater. Sol. Cells*, 185, 260–269. https://doi.org/10.1016/j.solmat.2018.04.029
2. Fong, K. et al. (2018). Phosphorus diffused LPCVD polysilicon passivated contacts with in-situ low pressure oxidation. *Sol. Energy Mater. Sol. Cells*, 186, 236–242. https://doi.org/10.1016/j.solmat.2018.06.039
3. Nie, S., Bonilla, R. S. & Hameiri, Z. (2021). Unravelling the silicon-silicon dioxide interface under different operating conditions. *Sol. Energy Mater. Sol. Cells*, 224, 111021. https://doi.org/10.1016/j.solmat.2021.111021
4. Liu, A. et al. (2018). Direct observation of the impurity gettering layers in polysilicon-based passivating contacts for silicon solar cells. *ACS Appl. Energy Mater.*, 1(5), 2275–2282. https://doi.org/10.1021/acsaem.8b00367
5. Ghembaza, H. et al. (2018). Optimization of phosphorus emitter formation from $POCl_3$ diffusion for p-type silicon solar cells processing. *Silicon*, 10, 377–386. https://doi.org/10.1007/s12633-016-9458-0
6. Suh, D. (2018). Efficient implementation of multiple drive-in steps in thermal diffusion of phosphorus for PERC solar cells. *Curr. Appl. Phys.*, 18(2), 178–182. https://doi.org/10.1016/j.cap.2017.11.024
7. Silva, J. A. et al. (2018). A one step method to produce boron emitters. *Phys. Status Solidi*, 215(17), 1701076. https://doi.org/10.1002/pssa.201701076
8. Lin, W. et al. (2020). Green-laser-doped selective emitters with separate BBr3 diffusion processes for high-efficiency n-type silicon solar cells. *Sol. Energy Mater. Sol. Cells*, 210, 110462. https://doi.org/10.1016/j.solmat.2020.110462
9. Hou, C. et al. (2018). Boron-rich layer removal and surface passivation of boron-doped p–n silicon solar cells. *J. Semicond.*, 39(12), 122004. https://doi.org/10.1088/1674-4926/39/12/122004
10. Kessler, M. A. et al. (2010). Charge carrier lifetime degradation in Cz silicon through the formation of a boron-rich layer during BBr_3 diffusion processes. *Semicond. Sci. Technol.*, 25, 055011. https://doi.org/10.1088/0268-1242/25/5/055001
11. Singha, B. & Solanki, C. S. (2016). Impact of a boron rich layer on minority carrier lifetime degradation in boron spin-on dopant diffused n-type crystalline silicon solar cells. *Semicond. Sci. Technol.*, 31, 35009. https://doi.org/10.1088/0268-1242/31/3/035009

12. Sheoran, M. et al. (2021). Photovoltaic waste assessment in india and its environmental impact. *J. Phys. Conf. Ser.*, 1849. https://doi.org/10.1088/1742-6596/1849/1/012003
13. Karthikeyan, L. et al. (2018). The management of hazardous solid waste in India: An overview. *Environ. – MDPI*, 5(9), 1–10. https://doi.org/10.3390/environments5090103
14. Kessler, M. A. et al. (2009). Characterisation and implications of the boron rich layer resulting from open-tube liquid source BBr_3 boron diffusion processes. *Conf. Rec. IEEE Photovolt. Spec. Conf.*, 6, 001556–001561. https://doi.org/10 .1109/PVSC.2009.5411365
15. Mohd Rais, A. R. et al. (2023). Non-destructive evaluation of toxic-less approach on emitter formation by water-based phosphoric acid for n-type silicon. *Silicon*, 15, 3091–3102. https://doi.org/10.1007/s12633-022-02231-3
16. Sinin, N. A. M. et al. (2023). The concentration factor on the mixture of Ag paste and H_3PO_4 solution as a dopant paste for contact formation in silicon solar cells. *J. Ovonic Res.*, 19(6), 681–694. https://doi.org/10.15251/JOR.2023.196.681
17. Huyeng, J. D. et al. (2018). Advancements in the utilization of screen-printed boron doping paste for high efficiency back-contact back-junction silicon solar cells. *2018 IEEE 7th World Conf. Photovolt. Energy Conversion, WCPEC 2018 - A Jt. Conf. 45th IEEE PVSC, 28th PVSEC 34th EU PVSEC*, 10–15 June 2008, 1544–1549. https://doi.org/10.1109/PVSC.2018.8547948
18. Zaidi, S. H. (2021). Dark current-voltage characterization. *Cryst. Silicon Sol. Cells*, 201–212. https://doi.org/10.1007/978-3-030-73379-7_5
19. Yu, C. et al. (2018). Recent advances in and new perspectives on crystalline silicon solar cells with carrier-selective passivation contacts. *Crystals*, 8(11), 430. https://doi.org/10.3390/cryst8110430
20. Aberle, A. G., Glunz, S. & Warta, W. (1992). Impact of illumination level and oxide parameters on Shockley-Read-Hall recombination at the Si-SiO2 interface. *J. Appl. Phys.*, 71, 4422–4431. https://doi.org/10.1063/1.350782
21. Eades, W. D. & Swanson, R. M. (1985). Calculation of surface generation and recombination velocities at the Si-SiO_2 interface. *J. Appl. Phys.*, 58, 4267–4276. https://doi.org/10.1063/1.335562
22. Kale, A. S. et al. (2019). Understanding the charge transport mechanisms through ultrathin SiO_x layers in passivated contacts for high-efficiency silicon solar cells. *Appl. Phys. Lett.*, 114, 083902. https://doi.org/10.1063/1.5081832
23. Novikov, A. (2010). Experimental measurement of work function in doped silicon surfaces. *Solid State Electron.*, 54(1), 8–13. https://doi.org/10.1016/j.sse.2009.09.005
24. Yan, D. et al. (2019). High efficiency n-type silicon solar cells with passivating contacts based on PECVD silicon films doped by phosphorus diffusion. *Sol. Energy Mater. Sol. Cells*, 193, 80–84. https://doi.org/10.1016/j.solmat.2019.01.005
25. Palmstrøm, C. J. (2001). Contacts for compound semiconductors: Ohmic type. *Encycl. Mater. Sci. Technol.*, 1581–1587. https://doi.org/10.1016/B0-08-043152-6/00282-5
26. Meier, D. et al. (1998). Self-doping contacts and associated silicon solar cell structures. *2nd World Conf. Photovolt. Sol. Energy Convers*, 1491–1494.

27. Porter, L. M., Teicher, A. & Meier, D. L. (2002). Phosphorus-doped, silver-based pastes for self-doping ohmic contacts for crystalline silicon solar cells. *Sol. Energy Mater. Sol. Cells*, 73, 209–219. https://doi.org/10.1016/S0927-0248(01)00126-X
28. Islam, R. & Saraswat, K. C. (2014). Metal/insulator/semiconductor carrier selective contacts for photovoltaic cells. *2014 IEEE 40th Photovoltaic Specialist Conference (PVSC)*, 285–289. https://doi.org/10.1109/PVSC.2014.6924915
29. Basher, M. K. et al. (2019). Effect of doping profile on sheet resistance and contact resistance of monocrystalline silicon solar cells. *Mater. Res. Express*, 29, 465705. https://doi.org/10.1088/2053-1591/ab1e8c
30. Bonilla, R. S. et al. (2020). Charge fluctuations at the Si-SiO_2 interface and its effect on surface recombination in solar cells. *Sol. Energy Mater. Sol. Cells*, 215, 1–15. https://doi.org/10.1016/j.solmat.2020.110649
31. Hiller, D. et al. (2018). Structural properties of Al-O monolayers in SiO_2 on silicon and the maximization of their negative fixed charge density. *ACS Appl. Mater. Interfaces*, 10, 30495–30505. https://doi.org/10.1021/acsami.8b06098
32. Hiller, D. et al. (2019). Deactivation of silicon surface states by Al-induced acceptor states from Al-O monolayers in SiO_2. *J. Appl. Phys.*, 125, 015301. https://doi.org/10.1063/1.5054703
33. Schmidt, J. et al. (2008). Surface passivation of high-efficiency silicon solar cells by atomic-layer-deposited Al_2O_3. *Prog. Photovoltaics Res. Appl.*, 20, 6–11. https://doi.org/10.1002/pip.823